

The Effect of Wear Groove on Vibration and Noise of Aircraft Brakes: Theoretical and Experimental Evidence

Kambiz Farhang, Soydan Ozcan and Peter Filip
Center for Advanced Studies
Department of Mechanical Engineering and Energy Processes
Southern Illinois University Carbondale

The goal of this paper is to delineate recent experimental evidence that the presence of conforming surface wear groove tends to stabilize the vibration and noise response of aircraft brakes. This finding is consistent with an earlier theoretical study in which the contact between Carbon-Carbon (C/C) composite brake disks were assumed to be visco-elastic and through this assumption it was found that the existence of conforming grooves results in increasing dynamic stability of brake disk interaction. Therefore, the presumption of visco-elastic contact for C/C brakes seems to agree with the experimental observation in a subscale dynamometer.

The present paper summarizes both theoretical analysis and the test results. In the tests C/C composites were heat treated for one hour at temperatures 1800°C and 2400°C, respectively. They were then subjected to frictional tests in a subscale aircraft brake dynamometer at 50 % relative humidity (RH) level. Coefficient of friction (μ), vibration and noise were recorded during simulated braking. The surface topography was determined after each sequence of friction tests. The nanohardness of fiber and matrix in bulk composite were measured using a nanoindenter. The hardness of fiber was found to be two times of that of the matrix for the samples heat treated at 2400°C as compared to the samples heat treated at 1800°C. The surface roughness (sRa) was measured as 1.96 μm for the sample heat treated at 2400°C after the 100% simulated normal landing energy conditions. The sample heat treated at 1800°C exhibited smoother friction surface (sRa=0.86 μm). During braking, μ varied by a factor of 2 or more which led to undesirable vibration.

Both the theoretical model and the tests results point to the same conclusion; existence of conforming grooves enhances dynamic stability of a disk pair, resulting in significant reduction in vibration and noise in braking.

Introduction

The implementation of analytical solutions of visco-elastic contact force equations allows the investigation of steady state of both contacts at rough flat and grooved surfaces. The interested

range of dimensionless asperity (micron bumps) radius of curvature, β , is from 100 to 140, corresponding to elastic contact. A dimensionless length parameter is the ratio of the length in question to the standard deviation of roughness asperity height distribution of the disk surface. In the steady state studies it is assumed that a rotor comes into contact with a stator disk in which the stator is considered to have normal and angular freedom due to flexibility of the connections. Assuming constant, the normalized separation of two disks, h , is varied from 3 to 4.5 and β from 100 to 140. The governing equations of the dynamic model were used to study the steady state relation between angular speed of upper disk and friction torque for the range of h and β .

Within the range of h and β , the critical parameters obtained from steady state analysis were then applied in simulink model to investigate the dynamic response of the system for both models.

As shown in Fig. 1, a mass-spring-damper system comprising an upper annular disk with a fixed angular velocity ($\dot{\phi}_1$) is supported by a lower initially stationary disk that is permitted to rotate about its central axis and translate along its axis (normal direction). The structural stiffness and damping in the normal direction are denoted, respectively, K_n and C_n while those for torsional motion are represented by K_{tor} and C_{tor} . The h_0 indicates the initial mean plane separation of two contacting rough surfaces due to an applied normal force, F_{na} . To simplify the study, the upper disk, m_1 , is assumed to be fixed in normal position after the application of a pre-load.

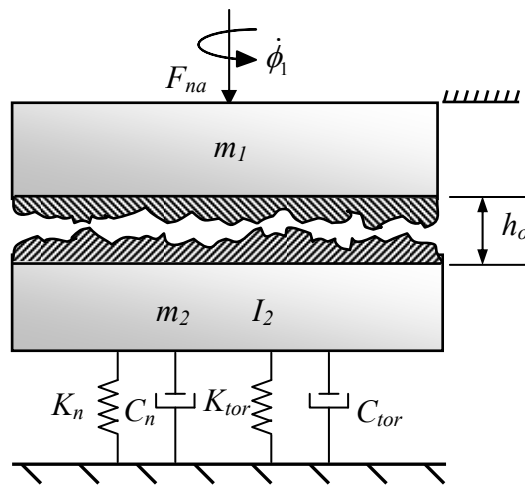


Figure 1 Schematic of the two-disk model

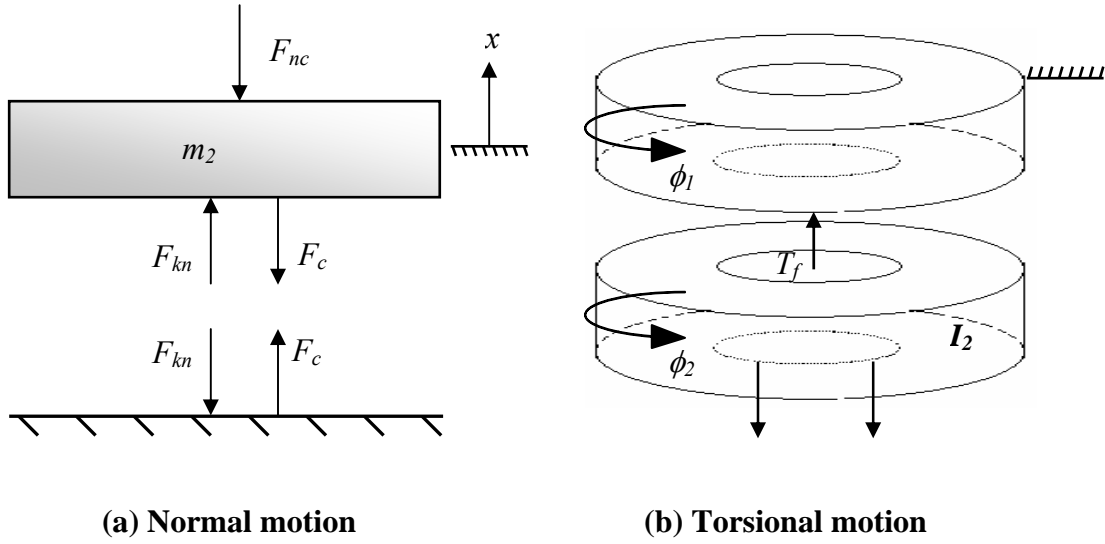


Figure 2 Free body diagram in (a) normal and (b) torsional motions

Referring to Fig. 2a, the governing equation of motion for normal can be expressed as

$$F_{kn} - F_{nc} - F_c = m_2 \ddot{x} \quad (1)$$

or

$$F_p - F_{nc} - K_n x - C_n \dot{x} = m_2 \ddot{x} \quad (2)$$

Where, F_p is the elastic force due to the pre-load, K_n and C_n are the structural stiffness and damping coefficient respectively. Function F_{nc} is the normal contact force between the two contacting rough surfaces contributed by additive visco-elastic contact components as

$$F_{nc} = F_{ne}^+ + F_{ne}^- + F_{nv}^+ + F_{nv}^- \quad (3)$$

The terms F_{ne}^+ and F_{ne}^- denote, respectively, the elastic normal contact forces at both positive and negative asperity interference slopes. F_{nv}^+ and F_{nv}^- are those contributed by rate dependent forces at both asperity shoulders,

Steady State Analysis for Contact of Nominally Flat Rough Surfaces

The steady state response of the two-disk system is investigated to study the relation between friction torque, T_f , angular speed of upper disk, $\dot{\phi}_1$, and the dimensionless average radius of summit curvature, β . The analysis involves the cases for different applied pre-load, F_p , and the dynamic factor, f_s , that dictates elastic contact contribution to friction torque.

In steady state condition, the angular speed of the stator, $\dot{\phi}_2$, and the normal velocity, \dot{h} , vanish. The governing equation of normal motion is

$$m_2 \ddot{x} = F_p - K_n x - C_n \dot{x} - 2C_{ne} A f_{ne} - 2C_{nvh} A_{nvh} f_{nvh} \dot{h} - 2C_{nvr} A_{nvr} f_{nvr} (\dot{\phi}_1 - \dot{\phi}_2) \quad (4)$$

At steady state, $\ddot{x} = 0$, $\dot{x} = 0$, $\dot{h} = 0$, reducing equation (1) to

$$F_p - K_n x - 2C_{ne} A f_{ne} - 2C_{nvr} A_{nvr} f_{nvr} (\dot{\phi}_1) = 0 \quad (5)$$

To find the angular speed of upper disk, $\dot{\phi}_1$, equation (5) can be recast as follows

$$\dot{\phi}_1 = \frac{F_p - K_n \sigma (h_0 - h) - 2C_{ne} A f_{ne3}}{2C_{nvr} A_{nvr} f_{nvr2}} \quad (6)$$

or, after substituting the appropriate approximate functions

$$\dot{\phi}_1 = \frac{F_p - K_n \sigma (h_0 - h) - 2C_{ne} A (319.956\beta - 115.254) h e^{-4.9h}}{2C_{nvr} A_{nvr} (-0.039\beta^2 + 13.976\beta + 285.238) h e^{-4.6h}} \quad (7)$$

The function f_{ne3} and f_{nvr2} were used since the interested range of h is from 3 to 4.5. The pre-load is basically the applied elastic normal force and it can be obtained as follows

$$F_p = 2C_{ne} A f_{ne3}(h_0) \quad 3 \leq h \leq 4.5 \quad (8)$$

or

$$F_p = 2 \left(\frac{8}{3} \frac{\pi}{\sqrt{2\pi}} E' \eta^2 \sigma^4 \sqrt{\beta} \right) \pi (R_o^2 - R_i^2) (319.956\beta - 115.254) h_0 e^{-4.9h_0} \quad (9)$$

where h_0 is obtained from the equations governing the rotation motion of the stator by setting $\dot{\phi}_2$ and \dot{h} to zero. The friction torque is found to be given by the following equation.

$$\begin{aligned}
T_f = & f_s C_a \left(\frac{8}{3} \frac{\pi}{\sqrt{2\pi}} E' \eta^2 \sqrt{\beta} \sigma^4 \right) \pi (R_o^3 - R_i^3) f_{te2} + \\
& C_b \left(\frac{4\pi}{\sqrt{2\pi}} \eta^2 \sqrt{\beta} E \eta_v \sigma^3 \right) \left(\frac{\pi}{2} \right) (R_o^4 - R_i^4) f_{tvr2} (\dot{\phi}_1)
\end{aligned} \tag{10}$$

A simple program was setup using Matlab software to solve the equations in steady state. First, the pre-load was chosen, and the initial values of normalized separation, h_0 , was calculated using equation (9). β was varied from 100 to 140 with step size of 0.5. The next step is to solve for $\dot{\phi}_1$ using equation (7). For a fixed pre-load, F_p , the corresponding h_0 is used in the equations while varying β from 100 to 140 and h from 3 to 4.5. Finally, the calculated $\dot{\phi}_1$ values are substituted into equation (10) to find the friction torque at the corresponding h and β .

Results of Steady State Analysis in Contact of Plain Rough Surfaces

First, cases resulting in stable and unstable dynamic response are presented. It is shown that it is possible for certain choice of surface parameters, axial load and material properties that the steady state response results in negative friction-sliding speed characteristics. Such negative slopes have been known to create instability in the dynamic response of two disks, manifested through noisy or vibration prone braking experience. The negative friction-torque is known as the Stribek effect.

Negative Rate-Dependent Friction (Stribek Effect)

The results of the steady state are plotted in graphs of friction torque versus angular speed of upper disk for various h and β . Figures 3 and 4 illustrate the results for potentially unstable or noisy case of braking since beyond a critical speed, the friction torque decreases with sliding speed. The various plots correspond to different values of dimensionless asperity radius of curvature.

The steady state investigations involved β from 100 to 140 with step size of 0.5, and h from 3 to 4.5 with step size of 0.02. Generally, as shown in the figures, the friction torque increases with sliding speed $\dot{\phi}_1$. This observation can be seen in all the figures at lower angular speed region. Throughout the entire range of $\dot{\phi}_1$, the increases in β will consistently lower the friction torque in all cases. The results suggest that higher speed and rougher surface (lower β) will generate more friction torque. Nevertheless, there is a critical point where friction torque

will reach a maximum value beyond which it will decrease as the angular speed (sliding speed) is increased further as shown in higher speed region in Figures 3 and 4. This is a significant behavior as negative slope in friction/speed curves can lead to dynamic instability.

The friction torque/speed curves shown in Figures 3 and 4 are reminiscent of friction speed curve in wet friction systems in which the curve shows a negative slope in the boundary and mixed (partial) lubrication regimes as shown in Figure 5. This phenomenon is known as Stribeck effect [1]. The friction torque also reaches a maximum value and shows negative slope region in the figures, this indicates that the material rate-dependent effect is a dominant factor that causes the negative slope curve. It is important to realize that the negative slopes are equivalent to negative damping coefficients that can affect dynamic instability of the system.

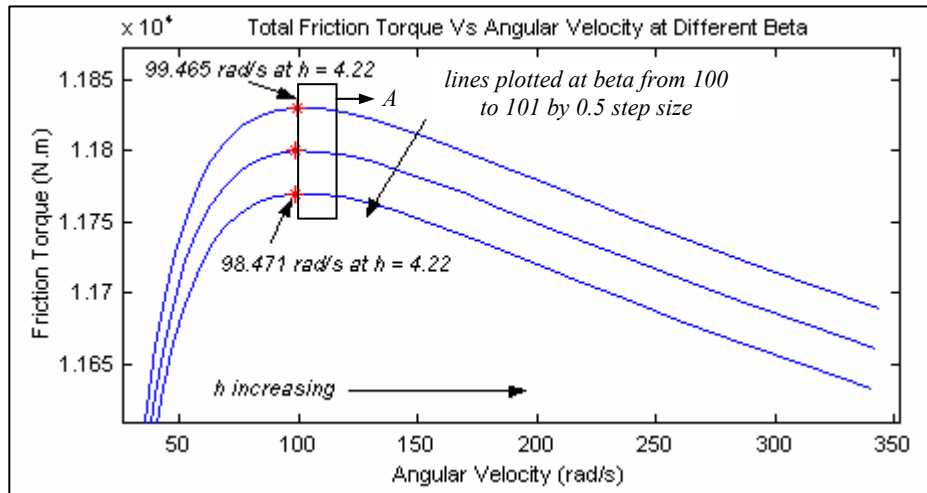


Figure 3 Friction torque vs. angular velocity at $\beta = 100$ to 101

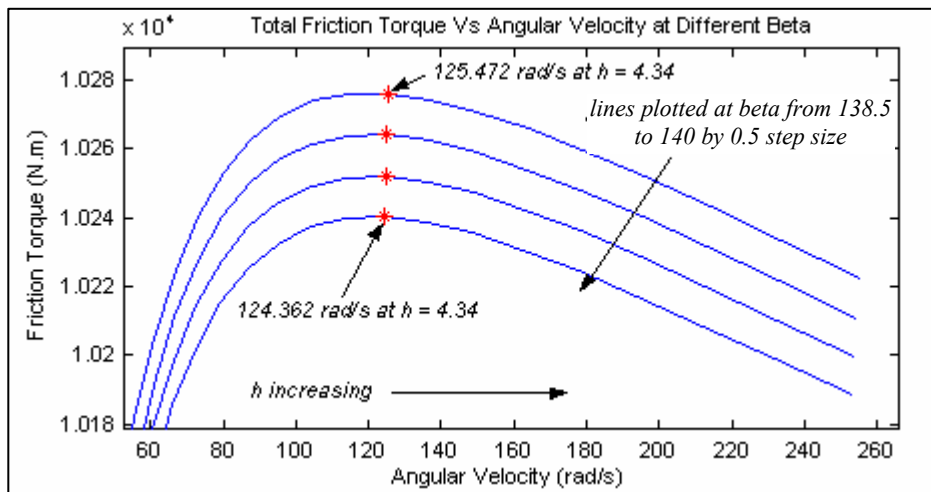


Figure 4 Friction torque vs. angular velocity at $\beta = 138.5$ to 140

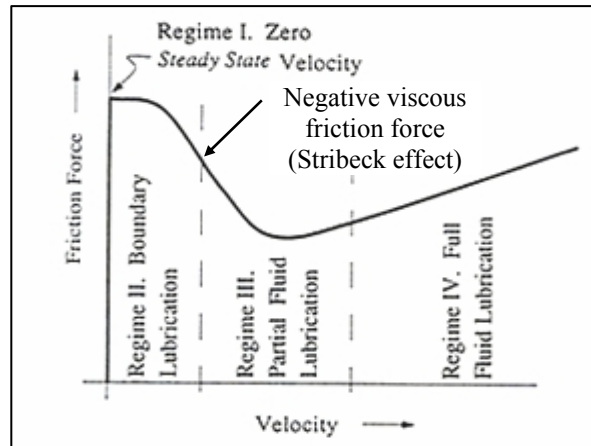


Figure 5 The generalized Stribeck curve (Armstrong, 1991)

Steady State Analysis of Two Disks in Contact with Single Wear Groove

The second dynamic model involves the interaction of a single grooved surface that accompanies its mating protrusion to establish conformal contact. To include the wear groove contact, a trapezoidal wear groove is implemented. Figure 6 illustrates the cross section view of the disk with a single trapezoidal wear groove and its geometrical parameters. The geometric variables involved five trapezoidal groove parameters, h_1 , h_2 , W_2 , θ_1 , and θ_2 as well as the radial distances, i.e. inner and outer radius of disk, R_i and R_o , the radial distance from disk center to the left and right shoulders, R_L , R_R , R_{bL} and R_{bR} . These parameters are used to calculate the nominal contact areas of a wear groove denoted as A^L , A^R and A^b for the left and right shoulders and the groove base, and A^{b1} and A^{b2} for the flat portions, as depicted in Fig. 7.

In accounting for the contact forces in a trapezoidal wear groove, one needs to consider the contact components at each face of the groove. When two disks interact in the normal motion, the elastic and rate-dependent contact forces at the left and right shoulders, base of the groove as well as the remaining flat disk portions of the disks contribute to disk's dynamic response. Figure 7 depicts the force components. The rate-dependent force components exist in the same direction as those elastic forces but these are not shown in the figure for the sake of clarity. Applying the assumptions mentioned in the previous section and following the free body

diagram in Fig. 2a along with the forces orientations depicted in Fig. 7, the governing equation of the dynamic model in normal motion can be expressed as follows

$$m_2 \ddot{x} = F_p - K_n x - C_n \dot{x} - 2 \left(F_{ne}^B + F_{ne}^L \sin \theta_1 + F_{ne}^R \sin \theta_2 \right) - 2 \left(F_{mvh}^B + F_{mvh}^L \sin \theta_1 + F_{mvh}^R \sin \theta_2 \right) - 2 \left(F_{mvr}^B + F_{mvr}^L \sin \theta_1 + F_{mvr}^R \sin \theta_2 \right) - \left(F_{te}^L \cos \theta_1 + F_{te}^R \cos \theta_2 \right) - \left(F_{tvh}^L \cos \theta_1 + F_{tvh}^R \cos \theta_2 \right) - \left(F_{tvr}^L \cos \theta_1 + F_{tvr}^R \cos \theta_2 \right) \quad (11)$$

$$I_2 \ddot{\phi}_2 + K_{tor} \phi_2 + C_{tor} \dot{\phi}_2 = f_s \left(T_{fe}^B + T_{fe}^L + T_{fe}^R \right) + \left(T_{fvh}^B + T_{fvh}^L + T_{fvh}^R \right) + \left(T_{fvr}^B + T_{fvr}^L + T_{fvr}^R \right) \quad (12)$$

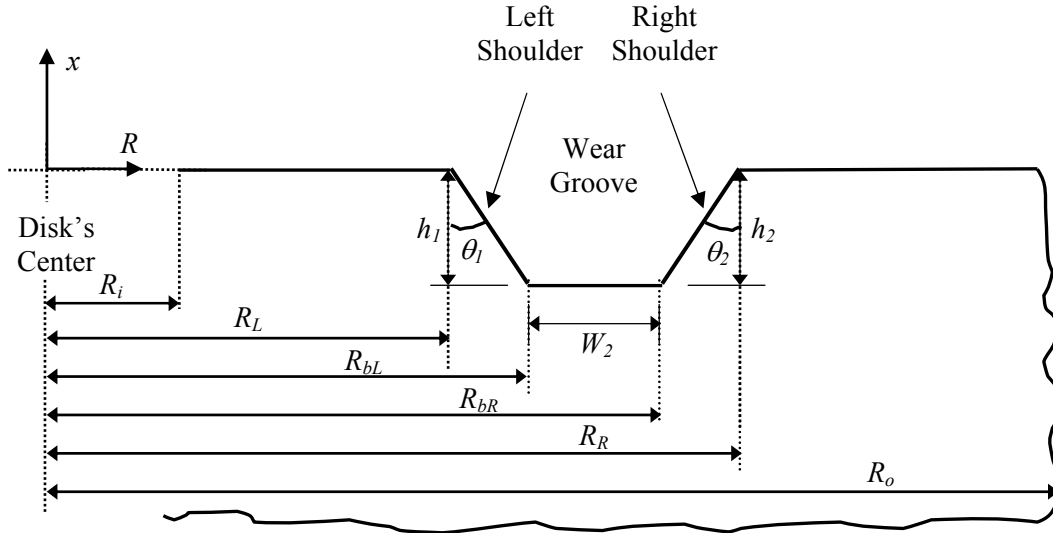


Figure 6 Cross-section view of a disk with single wear groove

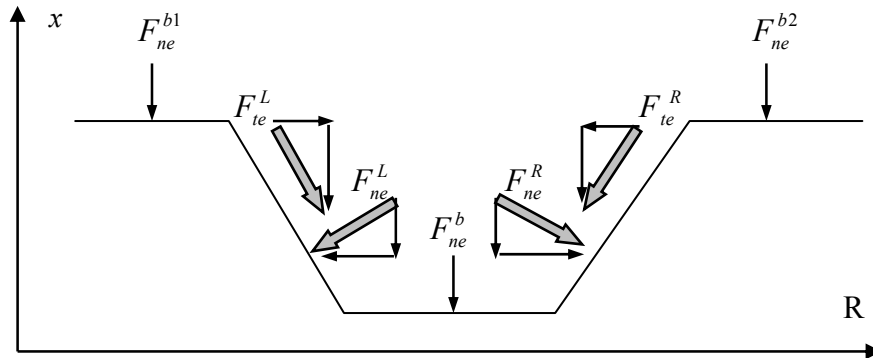


Figure 7 Contact components when two disks interacting in normal direction

The steady state analysis of disk with wear groove contact is studied in a similar manner to the flat rough surfaces. The steady state angular velocity of upper disk, $\dot{\phi}_1$, based on the governing equation of the dynamic model is given below

$$\dot{\phi}_1 = \left[F_p - K_n \sigma (h_0 - h) - 2 C_{ne} \left(f_{ne}^B (A_f^b + A_f^{b1} + A_f^{b2}) + f_{ne}^L \sin \theta_1 A_f^L + f_{ne}^R \sin \theta_2 A_f^R \right) - C_{te} \left(f_{te}^L \cos \theta_1 A_f^L + f_{te}^R \cos \theta_2 A_f^R \right) \right] / \left[2 C_{nvr} \left(A_f^b + A_f^{b1} + A_f^{b2} \right) f_{nvr}^B + 2 f_{nvr}^L \sin \theta_1 C_{nvr} A_f^L + 2 f_{nvr}^R \sin \theta_2 C_{nvr} A_f^R + f_{tvr}^L \cos \theta_1 C_{nvr} A_f^L + f_{tvr}^R \cos \theta_2 C_{nvr} A_f^R \right] \quad (13)$$

Where, pre-load

$$F_p = 2 \left(F_{ne}^B + F_{ne}^L \sin \theta_1 + F_{ne}^R \sin \theta_2 \right) + \left(F_{te}^L \cos \theta_1 + F_{te}^R \cos \theta_2 \right) \quad (14)$$

The friction torque function in this case is

$$T_f = f_s C_{te} \left(f_{te}^B \left(A_f^b + A_f^{b1} + A_f^{b2} \right) + f_{te}^L A_f^L + f_{te}^R A_f^R \right) + C_{tvr} f_{tvr}^B \left(A_g^b + A_g^{b1} + A_g^{b2} \right) \left(\dot{\phi}_1 \right) + f_{tvr}^L C_{tvr} A_g^L \left(\dot{\phi}_1 \right) + f_{tvr}^R C_{tvr} A_g^R \left(\dot{\phi}_1 \right) \quad (15)$$

As before the steady state analysis for the range of $\beta = 100$ to 140 and the h from 3 to 4.5 was performed. Equations (13) through (15) were solved using Matlab software.

Results of Steady State Analysis: Contact of Rough Surfaces with Wear Groove

The results of friction torque versus angular speed in steady state for two disks in contact that include contact between their conforming wear groove are shown in Figures 8 through 11. The negative slope region that appeared in previous study no longer exists in all the cases considered when wear groove is present. In the steady state analysis for contact of flat rough surfaces, it was illustrated that higher pre-load and the f_s factor will provide steeper negative slope in the curve, but this is not the outcome when wear groove contact is included as depicted in Figures 8 to 11. In all cases shown, the friction torque vs. sliding angular velocity show positive slope. Therefore, the effect of conforming groove is to remove instability that exists for plain surfaces. One then would expect a less noisy braking experience when conforming grooves are present. These grooves may be built into the design of the surface or brake material composition and processing could be design to ensure the occurrence of groove as a result of wear.

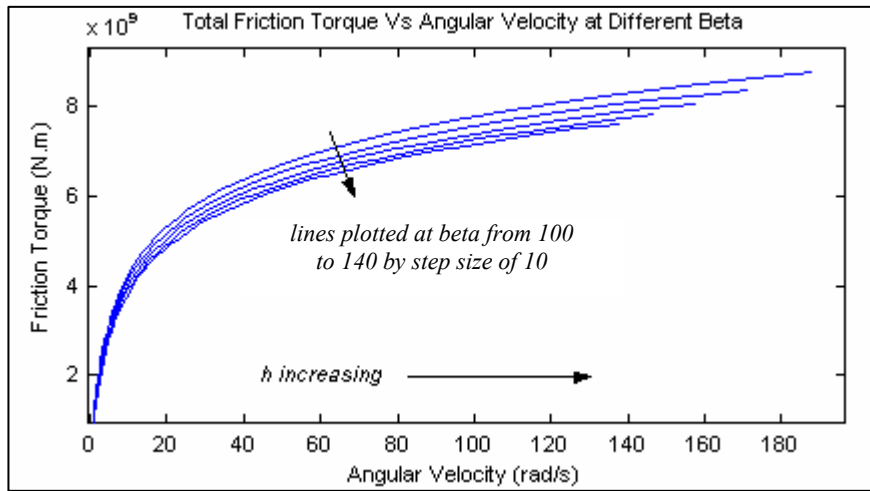


Figure 8 Friction torque vs. angular velocity at $\beta = 100$ to 140

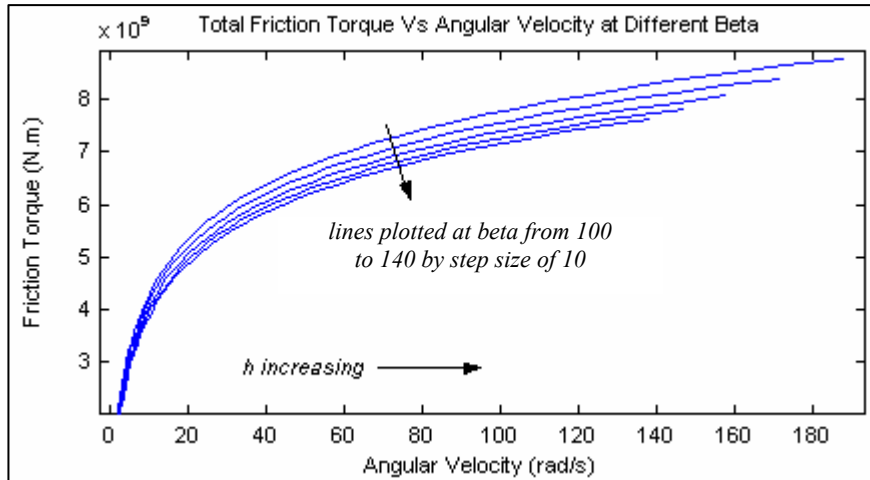


Figure 9 Friction torque vs. angular velocity at $\beta = 100$ to 140

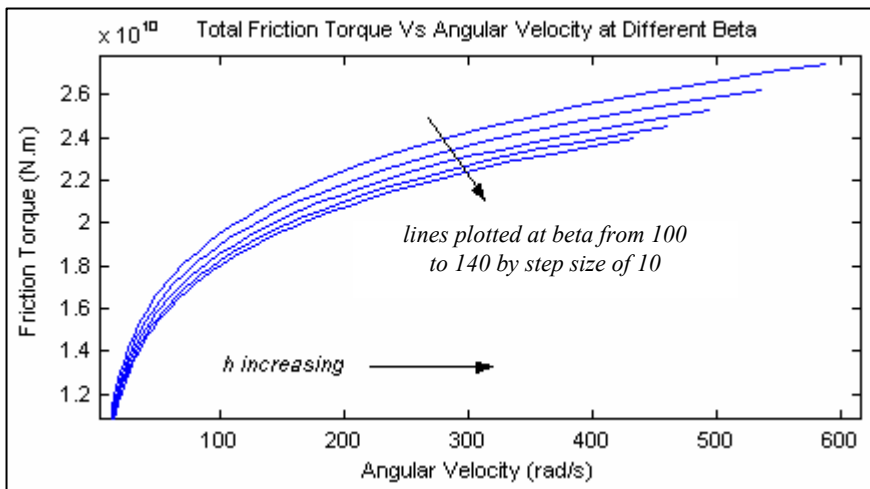


Figure 10 Friction torque vs. angular velocity at $\beta = 100$ to 140

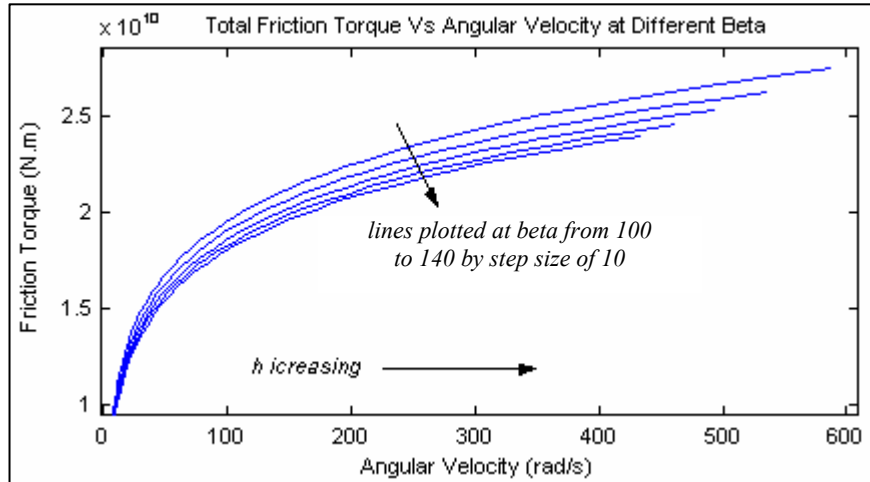


Figure 11 Friction torque vs. angular velocity at $\beta = 100$ to 140

In the next sections, the experimental investigation on braking noise and the effect of wear groove on noise are discussed and shown to agree with finding of the theoretical work discussed in here.

Experimental Investigation of Wear Groove Effect on Braking Noise

Brakes are designed to dissipate the kinetic energy into heat during the friction process. However, some of the kinetic energy turns into vibrations of the brake discs. The carbon/carbon composite friction materials (C/C) represent one of the most important elements of aerospace, military and higher end commercial vehicle brakes [1-5]. Since the 1960s, they have undergone significant development and improvement. Currently, PAN fiber reinforced rough laminar chemical vapor infiltrated carbon matrix composites are the commonly used materials in aircraft brake discs [4]. Vibration and noise is one of the top interests in the area of the C/C composite aircraft brakes [6]. Vibration damping is desirable for brakes which increases the reliability and comfort [7].

The commercially available fiber reinforced chemical vapor infiltrated (CVI) carbon matrix (CARBINEX 4000) aircraft brake material was used in this research. The composite was reinforced with multi-directional non-woven PAN-based carbon fibers. The C/C composites were heat treated at the temperature of 1800 and 2400°C, respectively. 1800°C and 2400°C heat treated composites will be referred to as CC18 and CC24, respectively.

The friction and vibration tests were performed using the Link Engineering sub-scale aircraft brake dynamometer (Model 2076, Plymouth, MI, USA) on C/C discs scaled down in

accordance to energy/mass ratio. The nominal outer and inner diameters of the ring specimens were 92.25 mm (3.75") and 69.85mm (2.75"), respectively. The friction tests were simulated at 4.5 and 100% of normal landing energy (NLE) and the relative humidity (RH) was controlled at 50%. The subscale aircraft brake dynamometer was operated in constant torque mode, the normal force varied in response to the current coefficient of friction, μ , to achieve the desired torque set point (2.041 kgf-m). For the period of the braking process, a number of parameters such as stop time: (7 to 34 sec), contact pressure (0.08 MPa to 0.35 MPa) and speed (202.8 km/h) were controlled. Three taxis performed at 4.5% NLE followed by one landing stop was repeated 50 times at 100% energy condition (200 braking events). The initial temperature of each test stop was set up at $T_0 = 50\text{ }^\circ\text{C}$ (120 °F) and the applied normal force ramp rate dF/dt was set up at 1780 N/s (400 lb/s). The μ , vibration and peak noise were recorded in real time.

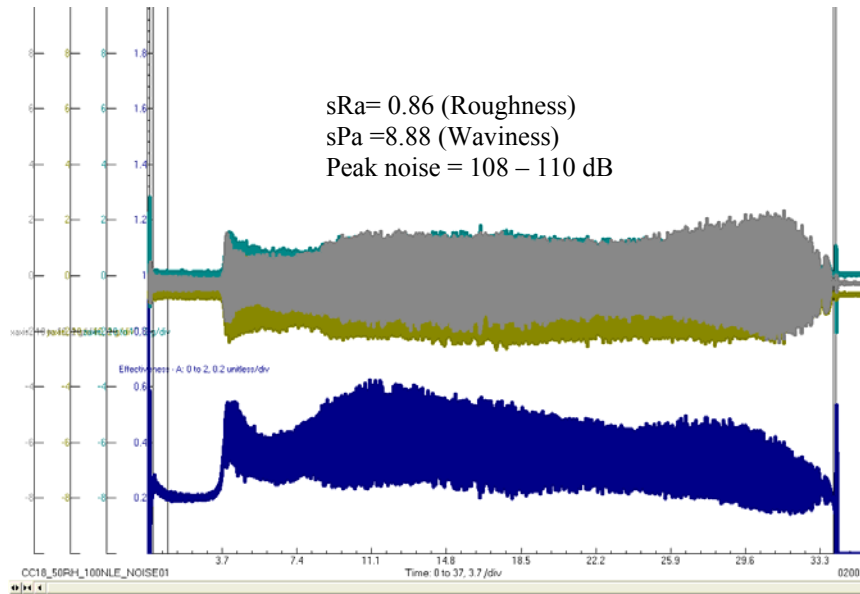
Surface parameters of the friction surface were measured after each testing sequence. A computer-controlled stylus profilometry manufactured by MAHR GmbH Company with a tip radius of 5 μm was employed. Vertical and lateral resolutions of the profilometry are 7nm and 19 nm, respectively. The nominal area of the measurement is 8 by 8 mm (256 traces) on both brake disc surfaces.

Nanohardness of each component of C/C composites was measured using an instrumented indentation technique. The indentation experiments were conducted at room temperature by a Nano Indenter® XP system MTS Nano Instruments, Knoxville, TN, USA, with Berkovich type diamond indenter. The nanoindenter was calibrated using a fused silica as standard before tests, allowing an evaluation of the analysis techniques. The displacement controlled and the continuous stiffness measurement (CSM) techniques were employed. Each component of C/C composite was probed 300nm depth and the method of Oliver and Pharr was employed in the evaluation of nano-hardness [8].

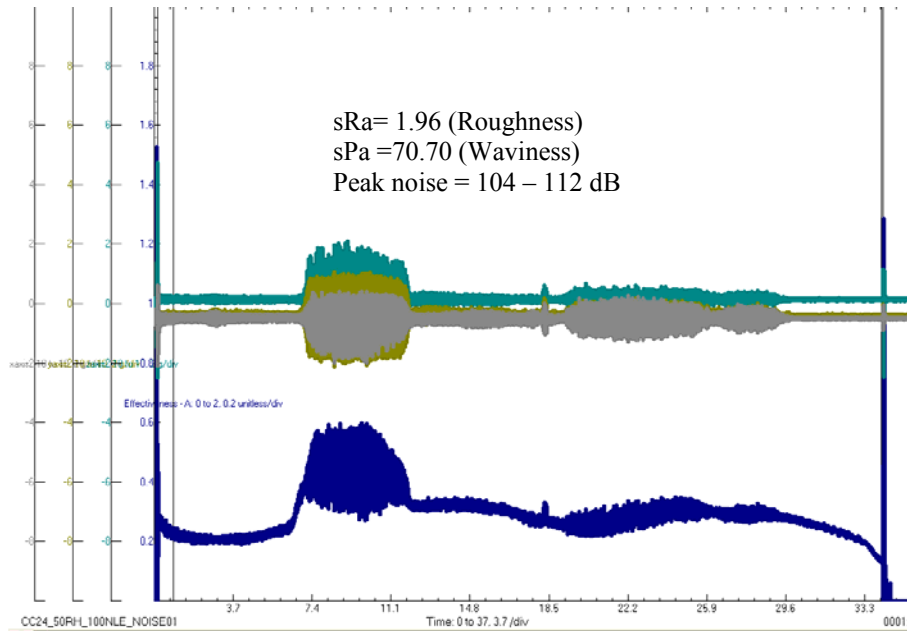
Results and Discussion

Characteristic μ and vibration of CC18 and CC24 during 100% NLE and 50% RH are plotted in Fig 12. Typically high vibration level started with the first transition of μ . This high vibration level continues with instability of the μ for the CC18 until the end of the each test. CC18 disks show no appreciable wear grooves, as seen from the profilometry results in Table 1. Figure 12(b) illustrates decreased level of vibration and noise with a more stable μ for CC24. Table 1 shows the appearance of a substantial wear groove in the CC24 disk pair. Thus CC24

which forms conforming wear grooves (Table 1) provides substantially reduced noise and vibration as depicted in Figure 12(b), whereas CC18 with no appreciable wear groove (Table 1) is significantly more noisy and vibration prone as shown in Figure 12(a). This finding is consistent with that predicted by the theoretical model discussed earlier.



(a)



(b)

Figure 12 Characteristic plot of three directional vibration and μ during simulated 100% NLE condition at 50% RH of CC18 (a) and CC24 (b).

Roughness and waviness of the friction surface after the 100% NLE and 50% RH are given in Table 1. The CC18 demonstrated a strong susceptibility to roughness after the 100% normal landing energy simulations, which is typically characterized by producing significant vibrations.

	CC18	CC24
sRa	0.86 μm	1.96 μm
sPa	8.88 μm	70.70 μm

Table 1. Surface parameters measured after the friction test at simulated 100% NLE and 50% RH level. (sRa and sPa are the roughness and waviness of the friction surface).

The measured nanohardness of CVI and PAN fiber are plotted in Fig. 13. Hardness of PAN fiber parallel to the fiber axial direction in CC24 is almost twice the elastic modulus of PAN fiber in CC18 at the same direction. Increasing the heat treatment temperature improves both the preferred orientation and the crystallinity. Thus, the basket weave microstructure of PAN fibers become harder to compressive loading in the fiber axial direction. It is expected that rough laminar CVI matrix turns to graphite-like microstructure with an increasing the heat treatment temperature. This type of microstructure is softer than the less developed microstructure as observed from the nanohardness of CVI as shown in Fig. 13. It is also observed that the higher hardness differences of the C/C composite components leads to the higher roughness of friction surface.

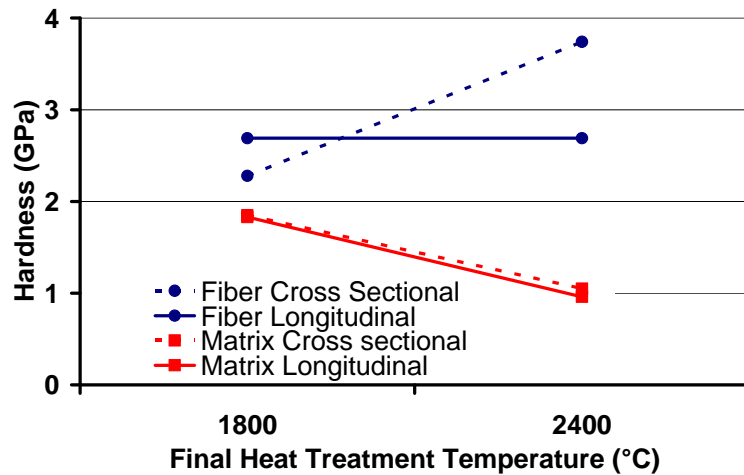


Figure 13 Nanohardnes of CVI matrix and the PAN fiber

Conclusion

This report has demonstrated that both theoretical and experimental investigation point to the stabilizing effect of conforming grooves in a disk pair. The theoretical portion of this investigation was first reported as a part of research at CAFS that focused on the effect of wear groove on vibration and noise in braking. This work was reported in one of the quarterly reports to the industry membership of CAFS.

Recent tests on C/C brake, as discussed in this paper, have supported the theoretical model that was developed earlier and suggest the following conclusions:

1. Conforming grooves in disk pair provide dynamic stability for a disk brake pair. This is supported by both model and sub-scale dynamometer tests.
2. It suggests that one of the mechanisms responsible for noise and vibration in C/C composite brakes is due to the rate-dependent properties of the brake material. Since the theoretical model employed visco-elastic properties of disk pair in dry contact yielded correct prediction of wear groove effect.
3. The finding suggests potential for C/C brake disk designs
 - a. Design surface texture with engineered conforming grooves
 - b. Design brake material development process so that the disk pair will form conforming grooves upon wear

A word of caution is in order. While conforming grooves provide dynamic stability and braking with reduced noise and vibration, misaligned or non-conforming grooves will have the opposite effect. Non-conforming grooves in fact destabilize a disk pair so that braking results in increased noise and vibration.

References

- [1] Armstrong-Helouvry, B., 1991, *Control of Mechanics with Friction*, Kluwer Academic Publishers.
- [2] Awasthi S, Wood JL. C/C Composite Materials for Aircraft Brakes. *Adv Ceram Mater.* 1988;3(5):449-51.
- [3] Byrne C, Wang Z. Influence of thermal properties on friction performance of carbon composites. *Carbon.* 2001;39(12):1789-801.
- [4] Ozcan S, Filip P. Microstructure and wear mechanisms in C/C composites. *Wear.* 2005;259(1):642-50.
- [5] Ozcan S, Krkoska M, Filip P. Frictional Performance and local properties of C/C composites. *Ceramic engineering and science proceedings.* 2005;26(8):127-38.
- [6] Farhang K, Lim AL. A Non-Phenomenological Account of Friction/Vibration Interaction in Rotary Systems. *Journal of Tribology.* 2006;128:103.
- [7] Faq C, Zone R. Damping characteristics of CVI-densified carbon-carbon composites. *Carbon.* 2000;38(13):1821-4.
- [8] Oliver WC, Pharr GM. Improved technique for determining hardness and elastic modulus using load and displacement sensing indentation experiments. *Journal of Materials Research.* 1992;7(6):1564-83.